LINEAR SYNCHRONOUS MOTOR CONTROL FOR AN URBAN MAGLEV

David W. Doll, *Robert Kratz, **Michael J. Newman
*** Allan B. Plunkett **** Robert D. Blevins
* General Atomics, 3550 General Atomics Court, San Diego, CA 92186, USA,
858 455 3888, david.doll@gat.com,
*858 455 2198, robert.kratz@gat.com,
**858 455 3477, michael.newman@gat.com
*** AC Drives Technology, 26280 S.W. Baker Road, Sherwood, OR 97140 USA
Tel: 503 625 5555 bmwalker@gte.net
**** Consultant, 3818 Pringle St., San Diego, CA 92103, USA
619 297 3827, rdblevins@aol.com

Keywords

Electro-dynamic Suspension (EDS), Urban MagLev, Linear Synchronous Motor (LSM), Permanent Magnet (PM), Pulse Width Modulation (PWM)

Abstract

A new concept in Urban Maglev transportation design is in the testing phase. The vehicle uses permanent magnets (PM) for both the electro-dynamic suspension (EDS) and linear synchronous motor (LSM) propulsion. Because of the 3D coupled non-linear velocity-dependent magnetic levitation, the LSM must provide stabilizing forces to the vehicle. To do this, Vector Control is used to modulate the inverter voltage, frequency and angle. The inverter angle is adjusted to maintain vertical stability. The controls architecture was developed and tested in a 2D simulation and verified in a 3D six dof dynamic model of the vehicle and guideway; the same magnetic levitation and LSM propulsion algorithms were used in both with the 2D simulation model providing the common control system. Control programming was implemented in C-code, which talks to the inverter pulse width modulation (PWM) card via an intermediate control box. The 2D simulation architecture provided the basis for implementing the control software design. Results from preliminary testing are discussed.

1 Background

The Urban MagLev system (low speed vehicles for inner-city service) now under development at General Atomics relies on an attraction assisted EDS for levitation and a LSM for propulsion. Both the on-board levitation and propulsion magnets are made from high-field NdFeB. This presents a challenge to the control system designer in that all six degrees of freedom (dof) are magnetically and dynamically coupled and are also coupled to the LSM propulsion. At stake is not only the basic operation of a vehicle but, because it is directed toward public transportation, the ride quality is of paramount importance [1].

The GA Urban MagLev uses simplified algorithms developed from 3D magnetic models (OPERA by Vector Fields) of the geometry in order to describe the forces and Simulink/Mathworks, and MSC Nastran Motion [2] to model the 2D and 3D dynamic operation, respectively. This paper describes the approach taken and includes a sample of the test vehicle simulation results. Included are results from static tests run in February 2004; dynamic operation started in September 2004 and is in progress at this time.

2 System Design

A description of the Urban Maglev is essential in understanding the controls design. A brief summary is presented, and a more complete description can be found in reference [3] and [4].

2.1 Full-Scale Commercial Vehicle and Guideway

Although the GA Urban Maglev is still in the prototype testing stage, a first deployment is in the planning stages at California University of Pennyslvania. The key feature of the attraction-assisted EDS is the use of PMs for both levitation and propulsion. The system is driverless, lending to central control. Vehicles may be operated singly or in trains. The guideway is elevated leaving full access to the space beneath for cross-traffic. Power systems are distributed along the wayside at intervals appropriate for block-switching, which keeps the LSM power demands to a minimum. A 2 minute headway ensures that the LSM duty factor is low with allowance made at stations for higher starting power demands. Figure 1 is an artist's concept of one fully deployed vehicle.

The levitation and propulsion components are located on either side of the guideway and are mechanically interlocked (Figure 2) with the LSMs directly above and in line with the levitation PM Halbach arrays and ladder track. Table 1 provides a summary of the key parameters for the fully deployed Urban MagLev system and test vehicle.

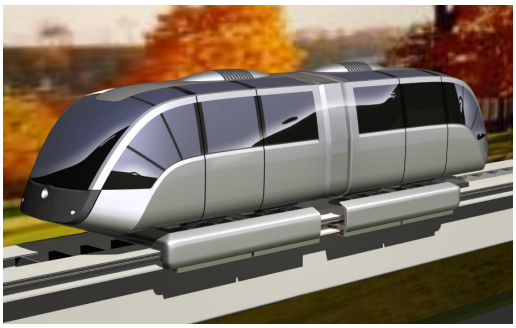

Figure 1. Urban Maglev Vehicle and Guideway

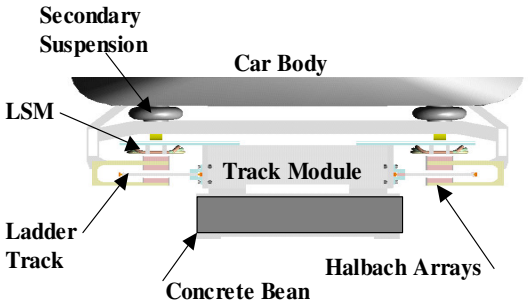

Figure 2. Vehicle-to-Guideway Arrangement

Table 1 Urban Maglev Specifications

System Parameter	Value for Full-Size Vehicle	Value for Test Vehicle
Levitation	PM Halbach array	PM Halbach array
Propulsion	PM LSM	PM LSM
Guidance	Attraction to LSM iron	Attraction to LSM iron
Permanent Magnets	NbFeB; Br=1.4 T; 50 mm sq	NbFeB; Br=1.4 T; 50 mm sq
Halbach Wave Length, λ	0.432 m	0.432 m
Number of PMs/ λ	M=8; 45 deg	M=8; 45 deg
Operation/safety	ATC (driverless)	ATC (driverless)
DC magnetic field to passengers	<1 Gauss	Measured
Speed/acceleration, maximum	160 km/hr (100 mph)	36 km/hr (22.5 mph)
Speed, average	50 km/hr (31 mph)	36 km/hr (22.5 mph)
Vehicle size	12 m x 2.6 m x 3 m	4 m x 2.6 m x 3 m
Vehicle weight	18 tonnes (100 passengers)	6–11.5 tonnes (no passengers)
Acceleration, max	1.6 m/s^2	1.6 m/s^2
Jerk, max	2.5 m/s^3	2.5 m/s^3
Grade	7% (design >10%)	Zero
Turn radius, minimum	25 m	50 m
Ride quality	ISO 2631 (1987)	Measured

2.2 Test Vehicle

A test vehicle has been built that duplicates without scaling half the actual vehicle described. Figure 3 shows the vehicle as it was installed onto the first guideway module. Preliminary checkout took place on this 15 m section of guideway, and went into full dynamic operation in September 2004 on a 120 m long track, which provides capability to accelerate to 10 m/s at 1.6 m/s^2. A 50 m radius was introduced midway of the track length in order to test the dynamics and control around a curve. Levitation, propulsion and guidance will validate the overall operation and control.

Figure 3. Urban Maglev Test Vehicle

2.3 Test Facility Power Systems

Propulsion power is supplied to the LSM from an inverter specifically designed by GA to handle the high peak current encountered as the vehicle accelerates through the drag peak encountered at 3 to 4 m/s. The inverter is three-phase five level and utilizes four half-bridges. Since the power is delivered into LSM load is voltage-limited, both a series delta and parallel Y connections will be tested to identify the lowest impedance and most scalable arrangement.

3 Dynamic Simulations Modeling

3.1 2D Simulation Description

Because of the coupled nature of the magnetics, it was necessary to construct a simulation of the Urban Maglev test system. Simulink/Matlab was selected as the computing platform. The simulation was developed for the test vehicle to meet that system's specific requirements, but modifications to scale to the full-sized commercialized system accounting for alignment features (grades, turns and station stops) are straightforward.

Four separate subsystems were used to describe the simulation: Control, Inverter, LSM and Vehicle. Each contains the particular algorithms best describing the hardware and software; Figure 4 shows the primary dependencies. A brief description of each subsystem follows.

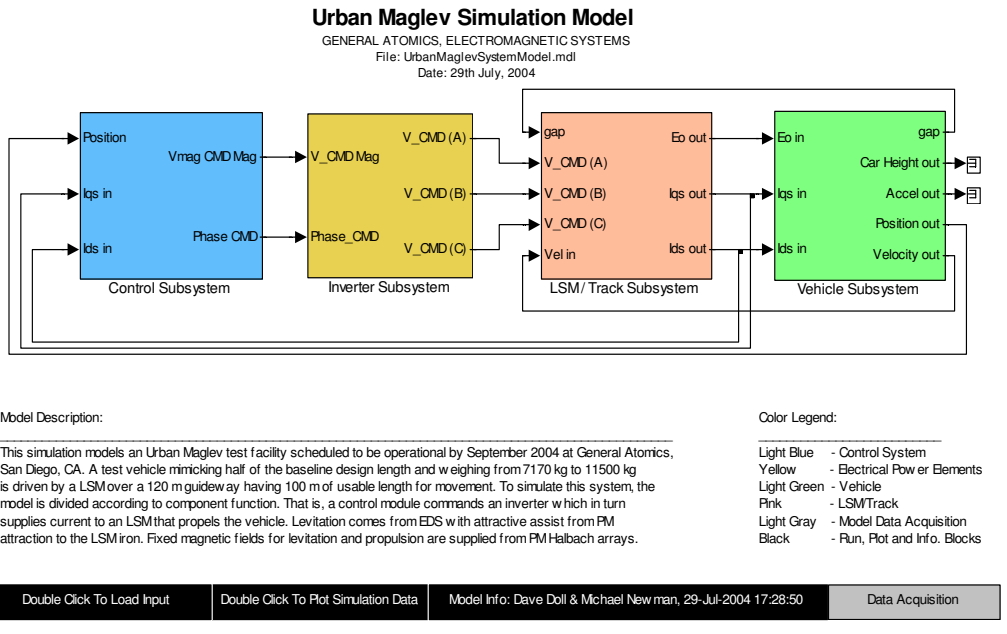

Figure 4. Matlab Simulink Model of the Urban Maglev Test Track System
with the Control Highlighted

Vehicle: The vertical force components are EDS levitation, LSM iron/PM attraction and LSM d-axis current, Ids, attraction/repulsion. For a given PM strength (nominally Br = 1.4 T) and geometry, EDS levitation forces depend on forward velocity and gap. PM/LSM iron attraction is exponential with gap and varies weakly with lateral displacement from centreline; d-axis current depends on motor angle. Thrust is derived from the q–axis current, which is sent with the d-axis current from the LSM.

LSM: This block calculates the current in the direct Id and quadrature Iq axes by vector transformations from the three phase voltages created by the inverter.

Inverter: The inverter takes the voltage magnitude and phase θ command coming from the Controls and converts them into three phases, A, B and C.

Controls: Vector control [5] is used for commanding the LSM drive currents. Unlike most PM LSMs, damping plates are not used to suppress oscillations. Instead, the voltage magnitude and angle are controlled to both suppress oscillations and provide a vertical force balancing mechanism to augment or suppress the attractive and levitating forces. Processing of the feedback signals is necessary before they are applied to the functions that generate the control signals to control to inverter, and thus the vehicle. This is done with filters.

3.2 3D Simulation Description

A 6 dof numerical simulation in NASTRAN Motion, a 3D modeling platform for solid body dynamics was used to model the MagLev test system. It included all the coupled magnetic forces derived for the 2D model plus the coupled dynamic forces in 6 dof, plus the lateral and vertical limiting guidance wheels that allow up to ±0.02 m travel. In order to test the simulated control system, the 3D NASTRAN simulation was coupled to the 2D Simulink controls simulation and run interactively. This gave the nearest approximation of the actual system practicable.

3.3 Magnetic Force Models

EDS lift and drag were calculated with a 3D current sheet model of the PM's B-field and verified against 3D calculations using OPERA. The interactions with the ladder track follows from Faraday's law. These calculations were performed for a series of gaps and velocities and subsequently subjected to a curve fit.

The form of the fit functions, i.e., the dependence on gap and velocity was taken from simple 2D theory. The fit coefficients adjust these functions to the three dimensional model. These coefficients incorporate the transition velocity and accounts for the footprint area, the track geometry and the 3D nature of the generating fields.

$$F_L(g_1,v) = N_{ski}\,(a_1 e^{-2k g_1} - a_2 e^{2k g_1}) \cdot \frac{1}{1+\left(\frac{a_3}{v}\right)^2} \quad \text{EQ1}$$

$$F_D(g_1,v) = N_{ski}\,(b_1 e^{-k g_1} - b_2 e^{k g_1})^2 \cdot \frac{\frac{b_3}{v}}{1+\left(\frac{b_3}{v}\right)^2} \quad \text{EQ2}$$

$$k_s(g_1,v) = N_{ski}\,2k(a_1 e^{-2k g_1} + a_2 e^{2k g_1}) \cdot \frac{1}{1+\left(\frac{a_3}{v}\right)^2} \quad \text{EQ3}$$

Coefficient	Value	Units	Error
a1	114.328	kN	0.04%
a2	7.335	kN	0.16%
a3	3.717	m/s	0.07%
b1	-10.889	sqrt(kN)	0.04%
b2	-2.740	sqrt(kN)	0.10%
b3	3.719	m/s	0.06%
Variable	**Value**	**Units**	**Definition**
k	14.544	1/m	2pi/Lambda
Lambda	4.320E-01	m	Wave length
FL		kN	EM Lift force
Fd		kN	EM Drag force
ks		kN/mm	Spring constant
g1		m	Mag. Levit. gap
v		m/s	Forward velocity

The LSM coupling to the propulsion Halbach arrays was more complicated. An attractive force exists between the PMs and the iron rails supporting the LSM coils which varies exponentially with the gap between them. Also, LSM operation off of a 90^0 motor angle produces an upward or downward force that varies with current, angle and exponentially with the LSM gap.

The coupled non-linear relationship describing the magnetic interaction between the LSM current and the Halbach arrays was also modelled in 3D OPERA (Vector Fields). Algorithms of the forces based on the linear dependence on current, exponential dependence on LSM gap and sinusoidal dependence on wave number were derived by curve fitting to 3D plots. This approach permitted calculating the dynamic forces in a simulation environment otherwise unapproachable if attempted completely in 3D. The functions and coefficients for thrust force, guidance force (active and passive) and lift forces (active and passive) are:

$$Th(d,g_3,\alpha) = \frac{N_{ski}}{4}\,(a_0 + a_2 \cdot d^2) \cdot \exp(a_g \cdot g_3) \cdot \frac{I_{peak}}{I_{norm}} \cdot \cos(\alpha) \quad \text{EQ4}$$

$$Ga(d,g_3,\alpha) = \frac{N_{ski}}{4}\,(ba_1 \cdot d + ba_3 \cdot d^3) \cdot \exp(ba_g \cdot g_3) \cdot \frac{I_{peak}}{I_{norm}} \cdot \sin(\alpha) \quad \text{EQ5}$$

$$Gp(d,g_3,\alpha) = \frac{N_{ski}}{4}\,(bp_1 \cdot d + bp_3 \cdot d^3) \cdot \exp(bp_g \cdot g_3) \quad \text{EQ6}$$

$$La(d,g_3,\alpha) = \frac{N_{ski}}{4}\,(ca_0 + ca_2 \cdot d^2) \cdot \exp(ca_g \cdot g_3) \cdot \frac{I_{peak}}{I_{norm}} \cdot \sin(\alpha) \quad \text{EQ7}$$

$$Lp(d,g_3,\alpha) = \frac{N_{ski}}{4}\,(cp_0 + cp_2 \cdot d^2) \cdot \exp(cp_g \cdot g_3) \quad \text{EQ8}$$

$$\alpha = \frac{x}{\lambda} \cdot 2\pi = x \cdot k \quad \text{EQ9}$$

Coefficient	Value	Unit
a0=	61.1509	kN
a2=	-0.0032	kN/mm^2
ag=	-0.0152	1/mm
cp0=	200.1756	kN
cp2=	-0.0747	kN/mm^2
cpg=	-0.0425	1/mm
ca0=	-66.9098	kN
ca2=	0.0088	kN/mm^2
cag=	-0.0138	1/mm
bp1=	-4.9915	kN/mm
bp3=	0.0022	kN/mm^3
bpg=	-0.0636	1/mm
ba1=	0.9485	kN/mm
ba3=	-0.0003	kN/mm^3
bag=	-0.0321	1/mm

Variable Definations

Th = Thrust

Ga = Guidance – active

Gp = Guidance – passive attraction

La = Lift – active

Lp = Lift – passive attraction

d = Lateral displacement

g_3 = LSM gap

α = Phase angle

3.4 Position Sensing

Position sensing emerged as a significant challenge. This was because the motor angle had to be controlled accurately, something not common in commercial train control. Simulations indicated the position had to be resolved within 18 mm in order to maintain stable operation. The vehicle vertical and lateral positions relative to the guideway are also monitored with laser position sensors in order to evaluate the 6 dof dynamic performance and validate the simulation models.
The forward position sensing system provides the angle information showing the absolute position of the magnets on the vehicle within a resolution determined by the position sensor resolution. Two resolutions used are 18 mm and 432 mm (motor wave length). This latter position resets the computer to avoid error build up.

3.5 Simulation Results

3.5.1 2D Simulation

Simulations were run for the full range of operating parameters with a focus on the effects of changes in the vehicle mass. The test vehicle mass can be varied from 6000 kg to 11500 kg with a primary mass of 4137 kg and the remainder in secondary structure and water ballast. Because of the 120 m track length and 50 m radius of the single curve, the velocity had to be limited to 10 m/s with a maximum acceleration of 1.6 m/s^2. The velocity profile used allowed full use of the track and was blended by limiting the jerk, set as an input parameter (1-1.6 m/s^3). The baseline for testing the simulation was chosen as 9000 kg since it lies midway between the weight limits. The test vehicle simulation parameters were: initial rest LSM gap g3 = 36.1 mm and corresponding levitation gap g1 = 17 - 18 mm. The initial gap g1 can be modified by starting on 5 mm or 10 mm shim beneath the start-off wheels.

Figure 5 shows the vehicle response to the baseline velocity profile (middle graph) and mass. The levitation gap in the upper graph shows lift-off delayed to later than it would otherwise be due to the use a shim beneath the start-off wheels. This was done to minimize the current draw while the vehicle passes through the magnetic drag peak at 3-4 m/s. The second line (violet) shows the response of the secondary or suspended part of the vehicle mass. It follows the primary closely but softens the dynamics for passenger comfort. The sudden lift-off occurs when the lift forces exceed the vehicle mass, and the resulting gap change reduces the magnetic drag correspondingly. As the vehicle slows and returns to its wheels, it does so in the same sudden manner. Wheels modeled with a high spring rate respond to the impact at their characteristic high frequency. Control was maintained through these rapid transients by a combination of the position observer and PI controllers in the control system.

The bottom graph in Figure 5 shows the vertical force balance through the 20 s simulation. At all times during levitation the sum of the lift forces must equal the vehicle mass. The LSM active vertical force is preset by the operator based on the vehicle mass and modulated to maintain the resultant force. A 9000 kg vehicle mass needs no downward or upward force to balance the forces for this gap.

The effect of position error on the thrust and normal force is indicated in the Figure 6. Note that changes in the motor thrust are small for relatively large position errors. However, the effect of a

position error on the normal force is more significant as the normal force could oscillate from a minus to plus value while the position jitters about zero.

The current, voltage and power show the effects of the magnetic drag. The force command increases the current in response the increased drag until the peak is reached. Thereafter, the current falls off until the vehicle reaches maximum speed. In the case of the test vehicle, this is limited by the track to 10 m/s. Time at this high current is only about 4 s, well within the inverter's transient capability and not a significant impact on the overall average power. Slow-down is dominated by the increased drag with reducing gap and added power required to maintain the 1.6 m/s deceleration rate.

3.5.2 3D Simulation

Simulation results showed stable operation over 120 m of straight track, but some difficulty through the 50 m turn. It was found that there is sufficient magnetic lateral guidance to maintain the Test Vehicle in a flat turn.

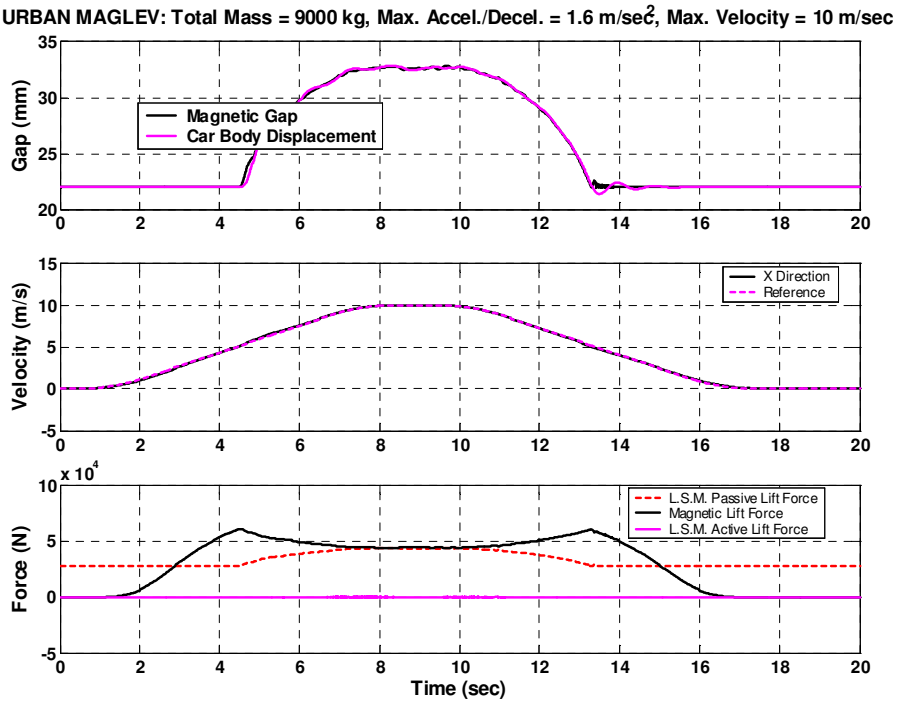

Figure 5. Gap and Force – Start-off Gap Raised to 27 mm with 5 mm Shim

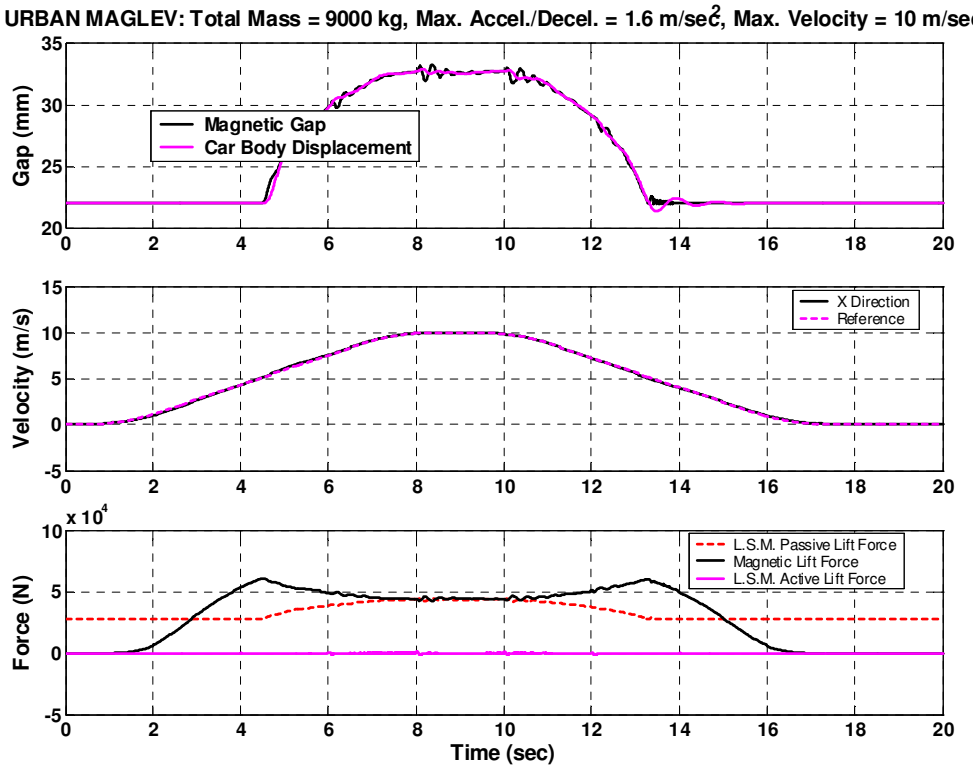

Figure 6. Simulation of Missing Position Location Pulses Every 2 seconds. Error Size: 20mm, offset duration: 50 ms, V_{max}: 10 m/s, $accel_{max}$: 1.6 m/s^2, mass: 9000 kg

4 Controls Design

Once the simulation was completed and satisfactory results obtained, the control logic and algorithms from it were reduced to C-code for implementation into the test facility power and sensing systems. The controls architecture used to construct the simulation also served to guide the implementation. The challenge was to implement only what was necessary without compromising the overall performance.

4.1 Architecture

The overall control architecture used in both the control simulation and implementation is shown in Figure 7. The process begins with the current command to the inverter, which comes from an initial magnetic gap estimate and the thrust requirement. These are summed with the measured Id and Iq to create the regulated current Ireg. From this, the voltages are calculated in the d and q axes, and the corresponding command angle calculated. This angle is summed with the motor angle to command the inverter via the PWM card. The Vd is adjusted by the vehicle weight to match a particular desired gap and the angle adjusted to achieve this gap. The key feedback data comes both from the inverter output and the position sensor. Current feedback is processed to create Idmeas and Iqmeas; the position sensor establishes velocity, acceleration and angle to the PWM via a position estimator that weights the estimates by a thrust/mass/acceleration comparison. The estimated velocity is then compared with the desired velocity to produce the thrust command via the IqCMD.

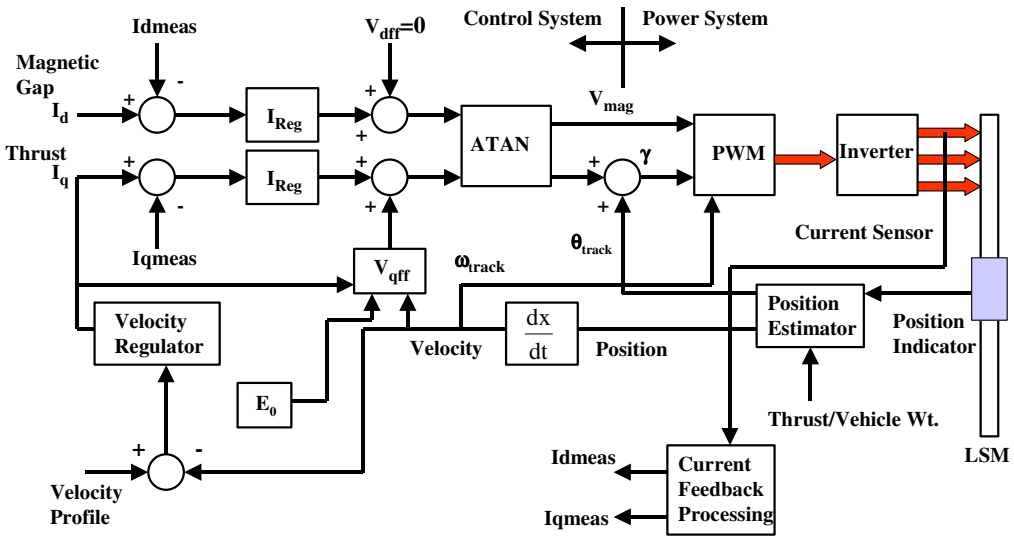

Figure 7. UML Control System Schematic

4.2 Approach to Implementation

Each of the function blocks that made up the simulated controls was reduced to a implementable form. This included processing of inverter voltages, currents and position data. The input signals to the control all require processing before being applied to the functions that generate the control signals to control to inverter, and thus the vehicle. The input signals consist of, inverter voltages and currents and the position sensor data. The data from the position sensor is transmitted to the control box using a serial fiber optic link. The actual data consists of steps in position. To make the position data useable in the control, the data is processed through a digital filter circuit, which provides smoothed data for position and velocity. The position signal and velocity signals are estimates, which will have some lag with respect to the actual data.

5 Test Results

Two sets of static tests were conducted on the vehicle. The first test measured the magnetic attraction of the PMs to the motor iron. Figure 8 shows the test results and the predicted values using equation EQ8. This agreement validated the static lift algorithm used in the controls.

"Locked rotor" tests were run to validate the LSM thrust force algorithms. With the vehicle anchored solidly to the guideway, the inverter was commanded to apply a fixed current at motor angles from 0^0 to 360° every 30°. The thrust was measured with load cells mounted along the thrust axis parallel to the track. Two levitation gaps were tested, 17 mm with no shim and 27 mm with a 10 mm shim beneath the start-off wheels. Figures 9 and 10 show the measured q-axis force with the calculated maximum values. These results showed excellent agreement with the predicted values calculated from EQ4.

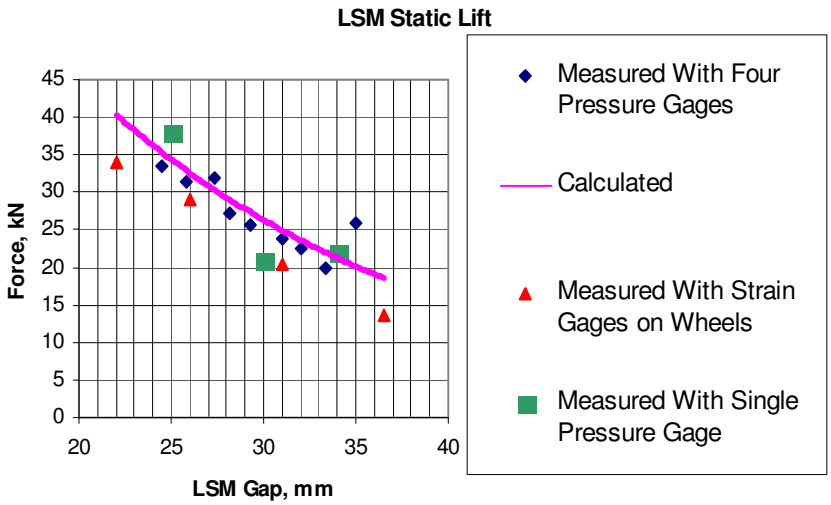

Figure 8. Static Lift Due to Attraction Between LSM Iron and PMs in the Halbach Arrays

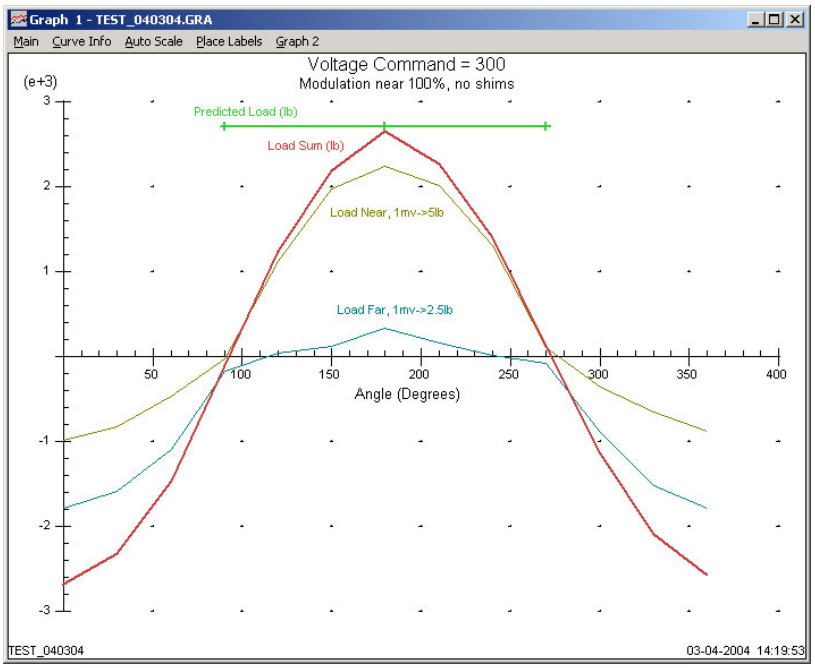

Figure 9. Locked-Rotor Test Results of the Maglev Vehicle with No Shims Under Start-off Wheels (17 mm Levitation Gap)

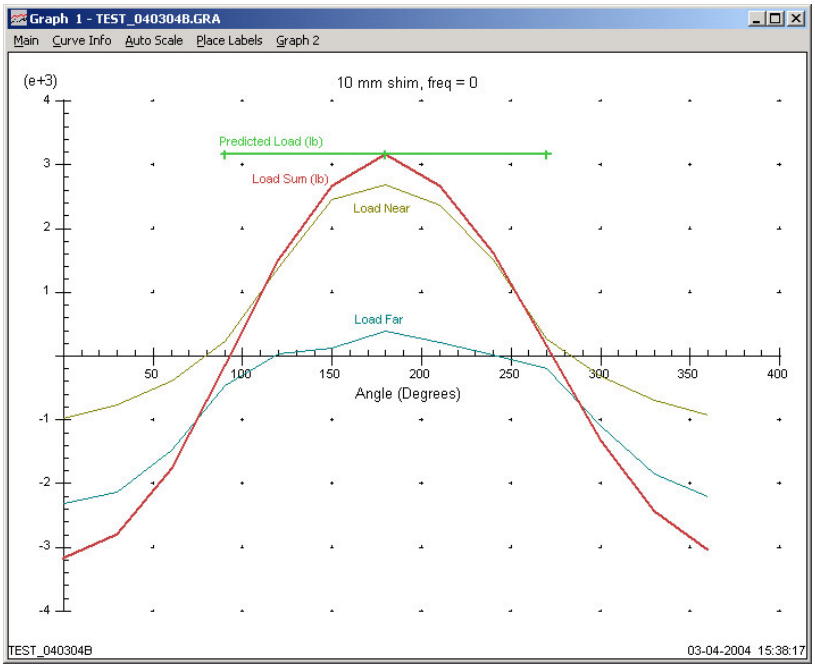

Figure 10. Locked-Rotor Test Results of the Maglev Test Vehicle with 10 mm Shims Under Start-off Wheels (27 mm Levitation Gap)

6 Conclusions

A control system has been developed for General Atomics' Urban Maglev test facility that can be scaled to apply to any alignment. Although the architecture used is fairly standard for transportation systems, the 6 dof coupled behavior required special algorithms describing the levitation, propulsion and guidance. These algorithms reduced the highly complicated 3D magnetics to a form usable in the control system. This understanding of the unique attraction assisted magnetic levitation gives confidence that the Urban Maglev will be successful in the remaining tests leading ultimately to commercialization.

7 Acknowledgements

This paper presents the results of a research effort undertaken by General Atomics under Cooperative Agreement No. CA-26-7025 to the Office of Research, Demonstration, and Innovation, Federal Transit Administration.

8 References

1. D. Doll, et al., "Ride Dynamics of General Atomics' Urban Maglev", Maglev 2002, Lausanne, Switzerland, September 4–8, 2002
2. MSC VISUAL NASTRAN, version 6.2, MSC software, Los Angeles, CA, 2000
3. Sam Gurol, Bob Baldi, and Richard L. Post, "Overview of the General Atomics Urban Maglev Program," Maglev 2002, Lausanne, Switzerland, September 4–8, 2002
4. Sam Gurol, Bob Baldi, "Status of the General Atomics Urban Maglev Program," Maglev 2004, Shanghai, China, October 24–29, 2004
5. D.W. Novotny and T.A. Lipo, "Vector Control and Dynamics of AC Drives", Oxford University Press, Great Clarendon Street, Oxford ox2 6dp, 2000